Controlled Synthesis of One-Dimensional Sb 2 Se 3 Nanostructures and Their Electrochemical Properties

ARTICLE *in* THE JOURNAL OF PHYSICAL CHEMISTRY C · AUGUST 2009

Impact Factor: 4.77 · DOI: 10.1021/jp902952k

6 AUTHORS, INCLUDING:

Jianmin Ma
Hunan University
94 PUBLICATIONS **1,703** CITATIONS
SEE PROFILE

Yaping Wang
Jiangsu University
37 PUBLICATIONS **492** CITATIONS
SEE PROFILE

Yijing Wang
Nankai University
131 PUBLICATIONS **1,761** CITATIONS
SEE PROFILE

Wenjun Zheng
Nankai University
112 PUBLICATIONS **2,298** CITATIONS
SEE PROFILE

Controlled Synthesis of One-Dimensional Sb_2Se_3 Nanostructures and Their Electrochemical Properties

Jianmin Ma,[†] Yaping Wang,[‡] Yijing Wang,[‡] Qing Chen,[†] Jiabiao Lian,[†] and Wenjun Zheng*,[†]

Department of Materials Chemistry, College of Chemistry, Nankai University, Tianjin 300071, People's Republic of China, and Institute of New Energy Material Chemistry, Engineering Research Center of Energy Storage & Conversion (Ministry of Education), Key Laboratory of Energy-Material Chemistry (Tianjin), Nankai University, Tianjin 300071, People's Republic of China

Received: April 1, 2009; Revised Manuscript Received: June 5, 2009

The size control of antimony triselenide (Sb_2Se_3) nanostructures has been achieved through a template-free hydrothermal route by simply adjusting the reaction temperature or the concentration of the reactants. Electrochemical measurements have shown that Sb_2Se_3 nanowires and mesorods possess higher initial hydrogen storage capacity than that of bismuth sulfide nanostructures (142 mAh/g) under normal atmosphere at room temperature. Interestingly, we have found that the morphologies of the Sb_2Se_3 had a noticeable influence on their capacity of electrochemical hydrogen storage. The result indicates that the Sb_2Se_3 nanowires have potential wide applications in hydrogen storage and high-energy batteries.

1. Introduction

One-dimensional (1D) nanostructures of different inorganic materials represent unique systems for exploring the dependence of various physical properties on dimensionality and size reduction, and have consequently been synthesized with an eye toward applications in various fields.[1−7] Inorganic nanowires are also expected to play a crucial role in future electronic and optoelectronic devices.[8] Since increasing attention has been paid recently on low cost, high throughput, high volume, and ease of production, various template-involved syntheses have developed as the method of choice for the synthesis of nanowires.[9] However, the main drawbacks associated with template-involved methods arise from the production and removal of templates, and thus there has been a great deal of interest in developing template-less strategies.

Group V−VI binary semiconductor compounds have received a great deal of attention due to their applications in television cameras with photoconducting targets, thermoelectric devices, optoelectronic devices, and IR spectroscopy.[10,11] Among these semiconductors, Sb_2Se_3, as a direct band gap semiconductor, has wide-ranging applications in solar selective and decorative coating, optical and thermoelectric cooling devices, due to its switching effects,[12] excellent photovoltaic properties, and high thermoelectric power.[13] In the past decades, inspired by their excellent characteristics, considerable efforts have been devoted to the fabrication of Sb_2Se_3 thin films. Amorphous and crystalline thin films of Sb_2Se_3 have been prepared by using a wide variety of thin film deposition techniques, including reactive pulsed laser deposition,[14] chemical bath deposition,[15] electrodeposition,[16] and vacuum thermal evaporation.[17−19] More recently, simple 1D Sb_2Se_3 nanostructures including nanorods, nanowires, and nanoribbons have been synthesized by various methods, such as a β-cyclodextrin-assisted solution process,[20] solvothermal routes,[21−25] a surfactant or polymer-assisted hydrothermal technique,[26−30] and a microwave-assisted method.[31,32] However, most methods employed organic solvents or templates to synthesize 1D Sb_2Se_3 nanostructures. Li et al.[33] reported the synthesis of Sb_2Se_3 nanorods under solvothermal condition; however, the growth temperature of pure Sb_2Se_3 nanorods should be above 130 °C. Therefore, it is still a hot issue to explore a facile route to the hydrothermal synthesis of 1D Sb_2Se_3 nanostructures without any template at low temperature.

Herein, we report a template-free hydrothermal method for the size-controlled synthesis of 1D Sb_2Se_3 nanostructures at low temperature, which is conducted by using active selenium resource originating from the reduction of Na_2SeO_3 by hydrazine hydrate. In addition, we have demonstrated that the Sb_2Se_3 nanowires can be electrochemically charged and discharged with the high capacity of 225 mAh/g at room temperature. It is found that the discharge capacity is sensitive to the size of Sb_2Se_3 products. Furthermore, the preparation and electrochemical studies of Sb_2Se_3 nanomaterials will offer great opportunities to explore the dependent relationship of novel properties of nanomaterials on their size. The obtained nanowires are expected to find wide applications in hydrogen storage and high-energy batteries.

2. Experimental Section

2.1. Chemicals. All of the chemicals were of analytical grade and were used as received. Aqueous solutions were prepared with distilled water.

2.2. Synthesis. In a typical synthesis, 0.01 g of $Sb(AcO)_3$ and 0.0085 g of Na_2SeO_3 were dissolved to 25 mL of distilled water, then 0.3 mL of hydrazine hydrate (80 wt %) was added under constant stirring. Subsequently, the resulting solution was transferred into a 30 mL Teflon-lined autoclave. The autoclave was sealed, heated, and maintained at 120 °C for 24 h. After the reaction was completed, the product was filtered, washed with dilute hydrochloric acid solution and distilled water several times, and then dried under vacuum after being heated at 220 °C for 20 min.

* To whom correspondence should be addressed. Phone: +86-22-23507951. Fax: +86-22-23502458. E-mail: zhwj@nankai.edu.cn.

[†] College of Chemistry, Nankai University.

[‡] Institute of New Energy Material Chemistry, Engineering Research Center of Energy Storage & Conversion (Ministry of Education), Key Laboratory of Energy-Material Chemistry (Tianjin), Nankai University.

10.1021/jp902952k CCC: $40.75
Published on Web 07/02/2009

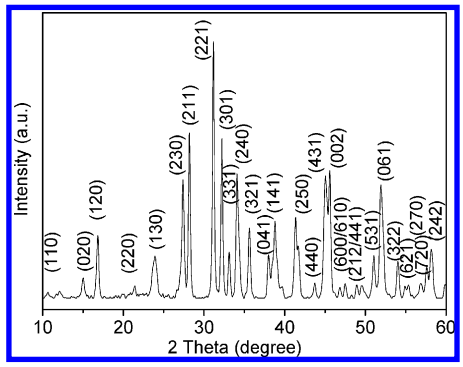

Figure 1. Typical XRD pattern of as-prepared nanowires.

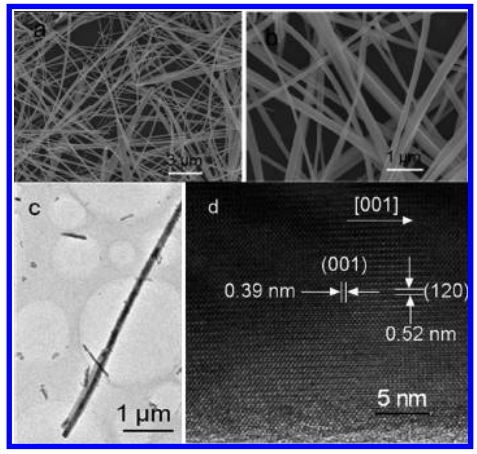

Figure 2. (a, b) Typical SEM images of as-prepared nanowires; (c) a part of an individual nanowire; and (d) corresponding HRTEM image of the individual nanowire.

2.3. Characterization. The X-ray diffraction (XRD) patterns of the products were recorded with a Rigaku D/max Diffraction System, using a Cu Kα source ($\lambda = 0.15406$ nm). The scanning electron microscopy (SEM) images were taken with a JEOL-JSM-6700F field emission scanning electron microscope (15 kV). The high-resolution transmission electron microscopy (HR-TEM) images were taken on a JEOL 2010 high-resolution transmission electron microscope performed at 200 kV. The specimen of HR-TEM measurement was prepared via spreading a droplet of ethanol suspension onto a copper grid, coated with a thin layer of amorphous carbon film, and allowed to dry in air.

2.4. Electrochemical Measurements. The electrochemical measurements were carried out following the method with slight modification. Briefly, the electrodes were constructed through mixing as-prepared Sb_2Se_3 powders with carbonyl nickel powders in a weight ratio of 1:3. Then, the powder mixture was pressed under 25 MPa pressure into a small pellet 10 mm in diameter and 1.5 mm thick. All of the experiments were performed in a three-electrode cell in 6 M KOH at 25 °C under normal atmosphere. The Sb_2Se_3 nanostructures were used as the working electrode, $Ni(OH)_2/NiOOH$ as the counter electrode, and Hg/HgO as a reference electrode. The Sb_2Se_3 nanostructures electrode was charged for 4 h at a current density after a 5 min rest. All of the electrochemical hydrogen storage experiments were carried out by using the Land battery system (CT2001A) at room temperature. The cyclic voltammetry measurements were carried out by an electrochemical workstation (CHI 660).

3. Results and Discussion

3.1. Structure and Morphology. X-ray powder diffraction (XRD) analysis was used to determine the structure of the nanowires. The results are shown in Figure 1. All the peaks in Figure 1 can be indexed to the orthorhombic phase of Sb_2Se_3 ($a = 11.63$ Å; $b = 11.78$ Å; $c = 3.985$ Å; JCPDS 15-0861). No impurities can be detected in this pattern.

The morphologies of nanowires were examined with a field-emission scanning electron microscope. Two SEM images of the product taken at different magnifications are shown in Figure 2, panels a and b. Figure 2a shows that the product contains a large quality of ultralong nanowires and several mesowires. As shown in Figure 2b, the mesowires are composed of several nanowires. The diameters of the products range from 80 to 100 nm. The morphology and structure of the Sb_2Se_3 nanowires is further investigated by TEM and HRTEM. Figure 2c shows a part of an individual Sb_2Se_3 nanowire, whose corresponding HRTEM image is shown in Figure 2d. The HRTEM image reveals that the nanowire is a single crystal and free from dislocation. The crystal planes, parallel and perpendicular to the rod axis, have spacings of 0.52 and 0.39 nm, which match well with the separations between the neighboring lattices of the (120) and (001) planes, respectively. This result further verifies that the preferential growth occurred along the [001] direction, which is coincident with that of Sb_2Se_3 nanoribbons and nanorods reported previously.[23,33]

3.2. Influences of the Experimental Parameters on the Morphology of the Products. The size of products significantly depends on the reaction temperature. When the reaction temperature is increased to 150 °C, rodlike products can be produced, as shown in Figure 3a. The resulting nanorods have a unique diameter of about 100 nm and a length of 1 μm. This could be explained by that higher reaction temperature changes the nanocrystal growth kinetics significantly and quenches nanowire elongation. Sigman et al.[34] found that high reaction temperature favored the formation of Bi_2S_3 nanorods rather than nanowires. Quan and co-workers[35] also observed that the size of Sb_2S_3 evolved from nanowires to microrods with the gradual increase of the reaction temperature. The growth habit of Sb_2Se_3 is similar to that of Bi_2S_3 and Sb_2S_3. In the present reaction

TABLE 1: Summary of the Size of Sb_2Se_3 Nanostructues Obtained under Various Conditions

	mass of the reactant (g)		vol of hydrazine reaction			
sample no.	$Sb(CH_3COO)_3$	Na_2SeO_3	hydrate (mL)	temp (°C)	morphology and diameter (nm)	FESEM image
S1	0.01	0.0085	0.3	120	nanowires (80−100)	Figure *2*a
S2	0.01	0.0085	0.3	150	nanorods (about 95)	Figure *3*a
S3	0.02	0.017	0.6	120	mesorods (400−800)	Figure *3*b
S4	0.005	0.0043	0.05	120	nanowires (80−120)	Figure SIa, *SI*
S5	0.005	0.0043	0.05	150	nanorods (100−200)	Figure SIb, *SI*
S6	0.005	0.0043	0.1	100	nanowires (about 60)	Figure SIc, *SI*
S7	0.005	0.0043	0.1	180	nanowires (100−140)	Figure SId, *SI*
S8	0.005	0.0043	0.1	200	nanrods (about 130)	Figure SIe, *SI*
S9	0.005	0.0043	0.1	220	nanrods (about 170)	Figure SIf, *SI*

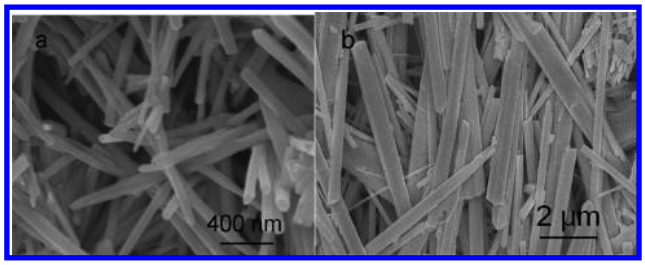

Figure 3. Typical SEM images: (a) nanorods and (b) mesonods.

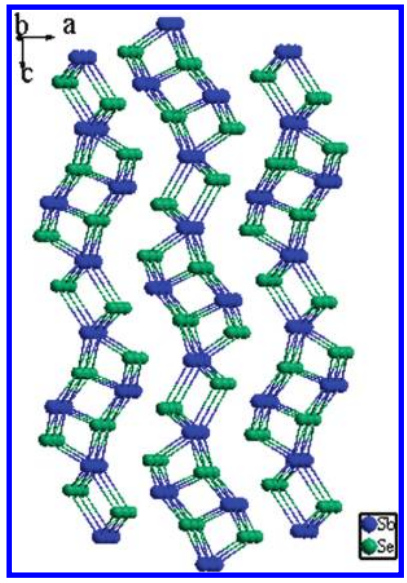

Figure 4. Crystal structure of Sb_2Se_3.

system, higher reaction temperature increases the rate of Sb_2Se_3 formation; the thermodynamic driving force for nucleation depletes the available Sb and Se needed to extend the nanostructures to large aspect ratios. Therefore, the reaction temperature plays an important role in the controlled formation of 1D Sb_2Se_3 nanostructures, and thus the size of 1D Sb_2Se_3 nanostructures could be adjusted by changing the reaction temperature in our reaction system.

Furthermore, the concentration of the reactants also has an important influence on the morphology of the final product. When the concentration of all reactants was increased twice, the Sb_2Se_3 mesorods were obtained, as shown in Figure 3b. The resulting mesorods appear to have diameters of 300−800 nm and lengths of about 9 μm. Under the present condition, the enhancement of the concentration of reactants could not lead to the outburst nucleation of Sb_2Se_3 on a large scale, thus the following reaction between Sb^{3+} and Se^{2-} proceeds on the existing Sb_2Se_3 nanorods naturally under the Sb−Se atom chain anisotropic and nonequilibrium growth conditions, and thus the

SCHEME 1: Possible Mechanism for the Electrochemical Hydrogen Storage of Sb_2Se_3

$$Sb_2Se_3 + H_2O + e \underset{\text{discharge}}{\overset{\text{charge}}{\rightleftharpoons}} (H_{ads} + Sb_2Se_3) + OH^-$$

diameters and lengths of Sb_2Se_3 increase until the Sb^{3+} and Se^{2-} in solution are exhausted. So, the mesorods could be obtained under high concentration of reactants. The result is similar to the phenomenon in the synthesis of Bi_2S_3 with use of low active S as the sulfur resource.[35] Therefore, the size of the 1D Sb_2Se_3 nanostructure could be adjusted by changing the concentration of the reactants in our reaction system.

In addition, 1D Sb_2Se_3 nanostructures with various aspect ratios were also obtained by adjusting the reaction temperature under constant reactant concentrations. Controlled experiments were conducted at different reaction temperatures: the morphologies of the product changed from nanowires to nanorods with the temperature increasing from 100 to 220 °C (Figure S1, Supporting Information), which further supported our deduction. To ascertain the influence factors on the morphology of Sb_2Se_3 products, the experimental parameters and their corresponding product morphologies are displayed in Table 1.

3.3. Proposed Formation Mechanism of Sb_2Se_3 1D Nanostructures. In a solution-phase synthesis without any organic additives or templates, the morphology of the final product is largely determined by the anisotropic nature of the building blocks. Therefore, studying the natural chemical character of antimony triselenide can help us understand the growth mechanism of these antimony triselenide nanowires. Sb_2Se_3 is a highly anisotropic semiconductor with layered structure parallel to the growth direction.[26,35] As demonstrated by Figure 4, it consists of infinite ribbonlike (Sb_4Se_6) polymers, linked together by intermolecular attraction between antimony and selenium atoms, which are parallel to the [001] (*c*-axis), which is also supported by the HRTEM observations. Therefore, the preferential growth into elongated crystals is determined by the anisotropic Sb−Se atom chain or layer structure of the orthorhombic Sb_2Se_3. Furthermore, kinetics factors, such as reaction temperature and the concentration of reactants, strongly influence the growth of 1D Sb_2Se_3 nanostructures. Therefore, various 1D Sb_2Se_3 nanostructures could be obtained by adjusting the kinetics factors under hydrothermal conditions.

3.4. Electrochemical Properties. Antimony triselenide with a lamellar structure is expected to exhibit excellent electrochemical hydrogen storage properties; for example, it was reported that isomorphic Bi_2S_3 with flowerlike nanostructures and disk-like nanorod networks electrochemically charge and discharge with the capacity of 142 mAh/g at a current density of 50 mA/g at room temperature.[37,38] Therefore, the electrochemical hydrogen storage behavior of the current Sb_2Se_3 nanowires was measured at a current density of 50 mA/g at

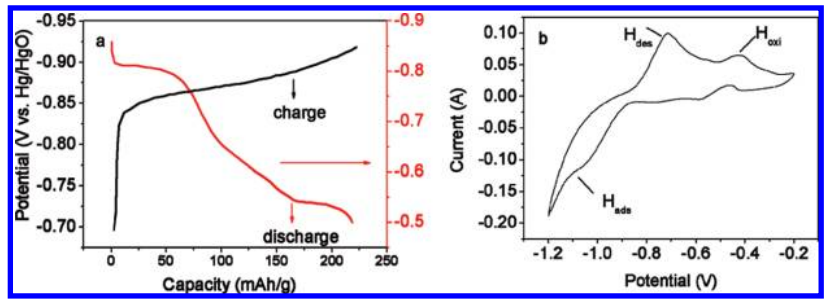

Figure 5. (a) Charge−discharge curve of the Sb_2Se_3 nanowires at 50 mA/g and (b) cyclic voltammogram of the Sb_2Se_3 nanowires in 6 M KOH at a sweep rate of 50 mV/s.

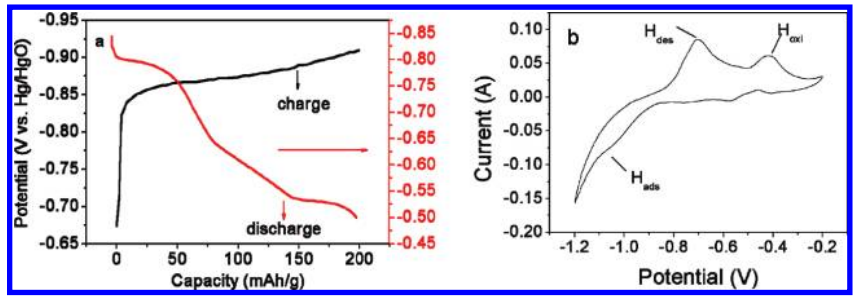

Figure 6. (a) Charge−discharge curve of the Sb_2Se_3 mesorods at 50 mA/g and (b) cyclic voltammogram of the Sb_2Se_3 mesorods in 6 M KOH at a sweep rate of 50 mV/s.

room temperature, and the charge−discharge curves displayed by the Sb_2Se_3 nanowire electrode are shown in Figure 5a. It can be seen that the charge−discharge voltage changes of Sb_2Se_3 nanowires as a function of capacity at a constant current density at room temperature. In the charge curve of Sb_2Se_3 nanowires, one obvious plateau of potential can be observed between 15 and 225 mAh/g. This indicates that one hydrogen adsorption site exists in the synthesized Sb_2Se_3 nanowires. In previous reports, a two-potential-plateau phenomenon in the charging curve was observed in nanostructures of other materials with a lamellar structure including flowerlike and nanorod network-like Bi_2S_3,[37,38] porous spongelike Ni_3S_2,[39] and $Cu(OH)_2$ nanobelt arrays.[40] According to Xie et al.,[37] the hydrogen was first adsorbed into the interstitial sites/pores between Bi_2S_3 nanorods in the network structures and then entered into the interlayers of Bi_2S_3 crystals. The first plateau should be attributed to the presence of complex structures. However, in our present work, there is only one plateau in the charge process of the Sb_2Se_3 nanowire electrode due to the presence of only simple Sb_2Se_3 wirelike structures. Therefore, it is assumed that the H is adsorbed into the interstitial sites among the $(Sb_4Se_6)_n$ chains, which is similar to the formation of the second plateau in complex structures of the above-mentioned materials.

Cyclic voltammograms (CVs) were also carried out to further investigate the electrochemical hydrogen adsorption−desorption behaviors of Sb_2Se_3 nanowires supported on the porous nickel substrate. In the CV of the Sb_2Se_3 nanowires, one broad reduction peak of hydrogen is obviously observed at ca. −1.09 V vs. Hg/HgO (close to the values of the Bi_2S_3 flowerlike pattern,[37] MoS_2 and BN nanotubes[41,42]), as displayed in Figure 5b. During the following anodic polarization, an anodic peak appears at −0.7 V, which is attributed to the desorption of hydrogen on the Sb_2Se_3 nanowires. As shown in Figure 5b, the hydrogen desorption peak can be observed prior to the hydrogen oxidation peak, indicating the possible existence of the strong chemisorption of hydrogen, similar to the observations and discussions for CVs of Bi_2S_3 flowerlike patterns[37] and BN nanotubes.[41] This also provides a complementary explanation for the above discussion on the charging process. As for the charge−discharge mechanism of Sb_2Se_3 nanowires, a simple scheme on the adsorption and release of hydrogen was tentatively displayed as shown in Scheme 1.

To study the size effect of Sb_2Se_3 on the capacity of electrochemical hydrogen storage, the charge−discharge curves of the synthesized Sb_2Se_3 mesorods as a function of capacity at a constant current density of 50 mA/g under normal atmosphere were measured and are shown in Figure 6a. For the Sb_2Se_3 mesorods sample, the value of the discharge capacity is 198 mAh/g, which is less than that of Sb_2Se_3 nanowires. This manifests that the size has exerted a noticeable influence on the electrochemical hydrogen storage ability of Sb_2Se_3 samples and also indicates that the size of Sb_2Se_3 products is a crucial factor for the high hydrogen storage capacity of Sb_2Se_3 nanowires. The corresponding cyclic voltammogram is shown in Figure 6b.

4. Conclusion

In summary, the size control of 1D Sb_2Se_3 nanostructures including nanorods, nanowires, and mesorods has been successfully realized through a simple hydrothermal route by adjusting only the reaction temperature or the concentration of the reactants. A possible growth mechanism is proposed to explain the formation of the 1D Sb_2Se_3 nanostructures from the viewpoint of crystal structure. The as-prepared Sb_2Se_3 nanowires have a higher hydrogen storage capacity, which will find potential wide applications in hydrogen storage and high-energy batteries. Furthermore, the hydrogen storage performance of Sb_2Se_3 nanostructures depending on their size will inspire more researchers to further focus on the morphology−properties relations.

Acknowledgment. This work was financially supported by the National Natural Science Foundation of China (20571044).

Supporting Information Available: Typical SEM images of as-prepared Sb_2Se_3 This material is available free of charge via the Internet at http://pubs.acs.org.

References and Notes

(1) Zhou, J.; Ding, Y.; Deng, S. Z.; Gong, L.; Xu, N. S.; Wang, Z. L. *Adv. Mater.* **2005**, *17*, 2107–2110.
(2) Pan, Z. W.; Dai, Z. R.; Wang, Z. L. *Science* **2001**, *291*, 1947–1949.
(3) Peng, X. G.; Manna, L.; Yang, W. D.; Wickham, J.; Scher, E.; Kadavanich, A.; Alivisatos, A. P. *Nature* **2000**, *404*, 59–61.
(4) Ouyang, L.; Thrall, E. S.; Deshmukh, M. M.; Park, H. *Adv. Mater.* **2006**, *18*, 1437–1440.
(5) Guiton, B. S.; Gu, Q.; Prieto, L.; Gudiksen, M. S.; Park, H. *J. Am. Chem. Soc.* **2005**, *127*, 498–499.
(6) Xu, D. S.; Xu, Y. J.; Chen, D. P.; Guo, G. L.; Gui, L. L.; Tang, Y. Q. *Adv. Mater.* **2000**, *12*, 520–522.
(7) Wang, W. Z.; Geng, Y.; Qian, Y. T.; Ji, M. R.; Liu, X. M. *Adv. Mater.* **1998**, *10*, 1479–1481.
(8) Lu, W.; Lieber, C. M. *J. Phys. D: Appl. Phys.* **2006**, *39*, R387−R406.
(9) Hurst, S. J.; Payne, E. K.; Qin, L. D.; Mirkin, C. A. *Angew. Chem., Int. Ed* **2006**, *45*, 2672–2692.
(10) Arivouli, D.; Gnanam, F. D.; Ramasamy, P. *J. Mater. Sci. Lett.* **1988**, *7*, 711–713.
(11) Case, T. W. *Phys. Rev.* **1917**, *9*, 305–310.
(12) Platakis, N. S.; Gatos, H. C. *Phys. Status Solidi A* **1972**, *13*, K1−K4.
(13) Black, J.; Conwell, E. M.; Sigle, L.; Spencer, C. W. *J. Phys. Chem. Solids* **1957**, *2*, 240–251.
(14) Xue, M. Z.; Fu, Z. W. *J. Alloys Compd.* **2008**, *458*, 351–356.
(15) Rodriguez-Lazcano, Y.; Pena, Y.; Nair, M. T. S.; Nair, P. K. *Thin Solid Films* **2005**, *493*, 77–82.

(16) Fernandez, A. M.; Merino, M. G. *Thin Solid Films* **2000**, *366*, 202–206.
(17) Arun, P.; Vedeshwar, A. G. *Thin Solid Films* **1998**, *335*, 270–278.
(18) Kumar, P.; Thangaraj, R. *Solid State Commun.* **2006**, *140*, 525–528.
(19) El-Sayad, E. A. *J. Non-Cryst. Solids* **2008**, *354*, 3806–3811.
(20) Batabyal, S. K.; Basu, C.; Sanyal, G. S.; Das, A. R. *Mater. Lett.* **2003**, *58*, 169–171.
(21) Wang, D. B.; Yu, D. B.; Shao, M. W.; Yu, W. C.; Qian, Y. T. *Chem. Lett.* **2002**, 1056–1057.
(22) Chen, M. H.; Gao, L. *Mater. Res. Bull.* **2005**, *40*, 1120–1125.
(23) Yu, Y.; Wang, R. H.; Chen, Q.; Peng, L. M. *J. Phys. Chem. B* **2006**, *110*, 13415–13419.
(24) Lu, J.; Han, Q. F.; Yang, X. J.; Lu, L. D.; Wang, X. *Mater. Lett.* **2008**, *65*, 2415–2418.
(25) Chang, H. W.; Sarkar, B.; Liu, C. W. *Gryst. Growth Des.* **2007**, *7*, 2691–2695.
(26) Wang, D. B.; Yu, D. B.; Shao, M. W.; Xing, J. Y.; Qian, Y. T. *Mater. Chem. Phys.* **2003**, *82*, 546–550.
(27) Ma, X. C.; Zhang, Z. D.; Wang, X.; Wang, S. T.; Xu, F.; Qian, Y. T. *J. Cryst. Growth* **2004**, *263*, 491–497.
(28) Xie, Q.; Liu, Z. P.; Shao, M. W.; Kong, L. F.; Yu, W. C.; Qian, Y. T. *J. Cryst. Growth* **2003**, *252*, 570–574.
(29) Chen, G. Y.; Dneg, B.; Cai, G. B.; Zhang, T. K.; Dong, W. F.; Zhang, W. X.; Xu, A. W. *J. Phys. Chem. C* **2008**, *112*, 672–679.
(30) Han, Q. F.; Chen, J.; Lu, J.; Yang, X. J.; Lu, L. D.; Wang, X. *Mater. Lett.* **2008**, *62*, 2054–2056.
(31) Zhao, C.; Cao, X. B.; Lan, X. M. *Mater. Lett.* **2007**, *61*, 5083–5086.
(32) Zhou, B.; Zhu, J. J. *Nanotechnology* **2009**, *20*, 085604−085609.
(33) Wang, J. W.; Deng, Z. X.; Li, Y. D. *Mater. Res. Bull.* **2002**, *37*, 495–502.
(34) Sigman, M. B., Jr.; Korgel, B. A. *Chem. Mater.* **2005**, *17*, 1655–1660.
(35) Quan, Z. W.; Yang, J.; Yang, P. P.; Wang, Z. L.; Li, C. X.; Lin, J. *Cryst. Growth Des.* **2008**, *8*, 200–207.
(36) Tideswell, N. W.; Kruse, F. H.; McCullouch, J. D. *Acta Crystallogr.* **1957**, *10*, 99–102.
(37) Zhang, B.; Ye, X. C.; Hou, W. Y.; Zhao, Y.; Xie, Y. *J. Phys. Chem. B* **2006**, *110*, 8978–8985.
(38) Li, L. S.; Sun, N. J.; Huang, Y. Y.; Qin, Y.; Zhao, N. N.; Gao, J. N.; Li, M. X.; Zhou, H. H.; Qi, L. M. *Adv. Funct. Mater.* **2008**, *18*, 1194–1201.
(39) Zhang, B.; Ye, X. C.; Dai, W.; Hou, W. Y.; Xie, Y. *Chem.—Eur. J.* **2006**, *12*, 2337–2342.
(40) Gao, P.; Zhang, M. L.; Niu, Z. Y.; Xiao, Q. P. *Chem. Commun.* **2007**, 5197–5199.
(41) Chen, J.; Kuriyama, N.; Yuan, H.; Takeshita, H. T.; Sakai, T. *J. Am. Chem. Soc.* **2001**, *123*, 11813–11814.
(42) Chen, X.; Gao, X. P.; Zhang, H.; Zhou, Z.; Hu, W. K.; Pan, G. L.; Zhu, H. Y.; Yan, T. Y.; Song, D. Y. *J. Phys. Chem. B* **2005**, *109*, 11525–11529.

JP902952K